

SELF-SCULPTING OF MELTING ICE BY NATURAL CONVECTION

Scott Weady

INTRODUCTION

Glaciers and icebergs exhibit fascinating morphology, including structures such as caverns, spikes, and wave-like patterns known as scallops (Figure 1). These features are a signature of the coupling between flow and shape: as ice melts into water, it produces and modifies flows, which non-uniformly melt the ice surface. The surface recedes, and the process repeats. This feedback mechanism is not limited to ice alone. In fact, melting belongs to a much broader class of problems known as moving boundary problems, which encompass a variety of geophysical processes such as dissolution, erosion, solidification, and ablation [1] [2].



FIGURE 1: Overturned icebergs reveal complex morphology including scalloping (a),(d) and spikes (b),(c).

A unique property of melting ice that separates it from other moving boundary problems is that water is densest a few degrees above its freezing point, a familiar consequence of which is that ice floats. This property, commonly referred to as the density inversion, generates exotic flow patterns distinct from those arising in classical convection [3] [4].

In this report, we examine how the density inversion influences the shape of melting ice. We consider the effects of natural convection alone, that is, flow driven solely by density variations. Our approach in-

volves experimental, numerical, and theoretical techniques that work together to form a broader picture of the complex shape dynamics.

We first theoretically formulate the melting problem and its moving boundary conditions, and then describe our experimental, numerical, and analytical approaches. We conclude with an outlook on further applications and discuss the significance of moving boundary problems in the context of climate change.

Equations of motion

Moving boundary problems are typically formulated as partial differential equations (PDEs) in a domain whose boundary is an unspecified function of time, meaning the boundary itself is part of the solution. To fully describe the solution, we then need both boundary conditions for the PDE as well as an evolution equation for the moving interface.

As a starting point, a simple model for the density of water as a function of temperature T is

$$\rho(T) = \rho_*(1 - \beta(T - T_*)^2), \quad (1)$$

where $T_* \approx 4^\circ\text{C}$ is the temperature of maximum density ρ_* , and β is a thermal expansion coefficient [5]. The full equations of motion with variable density are both numerically and analytically challenging, so to simplify matters we make the *Boussinesq approximation*, which neglects all density variations except those that multiply gravity. Using this approximation and a standard non-dimensionalization procedure, we arrive at the dimensionless Boussinesq equations,

$$\frac{\partial \mathbf{u}}{\partial t} + \mathbf{u} \cdot \nabla \mathbf{u} = \text{Pr}(-\nabla p + \Delta \mathbf{u} + \text{Ra} \theta^2 \hat{\mathbf{z}}), \quad (2a)$$

$$\nabla \cdot \mathbf{u} = 0, \quad (2b)$$

$$\frac{\partial \theta}{\partial t} + \mathbf{u} \cdot \nabla \theta = \Delta \theta. \quad (2c)$$

Here $\mathbf{u}(\mathbf{x}, t)$ is the fluid velocity, $p(\mathbf{x}, t)$ is the pressure, and $\theta(\mathbf{x}, t) = (T(\mathbf{x}, t) - T_*) / (T_\infty - T_0)$ is the deviation from the temperature of maximum density, normalized by the difference in the far-field temperature T_∞ and the melting temperature $T_0 = 0^\circ\text{C}$. The first two equations, (2a) and (2b), are the famous Navier-Stokes equations, which describe the incompressible velocity field within the fluid, while the last

equation (2c) describes the evolution of the temperature field.

The Boussinesq equations depend on two dimensionless parameters called the Rayleigh number $Ra = g\beta(T_\infty - T_0)^2 L^3 / \nu K$ and the Prandtl number $Pr = \nu / K$, where g is acceleration due to gravity, L is the length scale, ν is the viscosity, and K is the thermal diffusivity. The Rayleigh number, which is proportional to L^3 , characterizes how turbulent the flow is, while the Prandtl number describes the separation of time scales between the temperature and velocity fields. For water, the Prandtl number is roughly constant with $Pr = 12$, while the Rayleigh number ranges from 10^6 on laboratory scales to 10^{12} on geophysical scales.

In this system the temperature and velocity fields are coupled through the last term in Equation (2a), $Ra\theta^2 \hat{\mathbf{z}}$, which describes the buoyancy force. Here larger values of $Ra\theta^2$ indicate lighter fluid, while smaller values indicate denser fluid. Though this term is always positive, it can be shown that the pressure comes into *hydrostatic balance* with the far-field temperature, meaning that only the relative force $Ra(\theta^2 - \theta_\infty^2)$ acts on the fluid.

The Stefan condition

Classically, melting boundaries are described by the Stefan condition, which says the melt rate is proportional to the temperature gradient along the surface,

$$\tilde{v}_n = St \frac{\partial \theta}{\partial n}.$$

Here \tilde{v}_n is the (dimensionless) normal velocity of the interface and $St = c_p(T_\infty - T_0)/\mathcal{L}$ is the Stefan number, where c_p is the heat capacity and \mathcal{L} is the latent heat of fusion. The Stefan number can roughly be characterized as the energy required to melt a unit mass of ice. In addition to the Stefan condition, ice is governed by the Gibbs-Thomson effect, which causes regions of high curvature to melt faster. To leading order, this can be incorporated into the boundary condition by modifying the normal velocity as

$$v_n = \tilde{v}_n(1 + \gamma\kappa), \quad (3)$$

where κ is the surface curvature and γ is a material constant. With the Boussinesq equations (2a)–(2c) and the Stefan condition (3), we have a complete analytic description of the moving boundary problem.

EXPERIMENTS AND SIMULATION

Our study of melting ice is driven by table-top experiments and numerical simulation which motivate

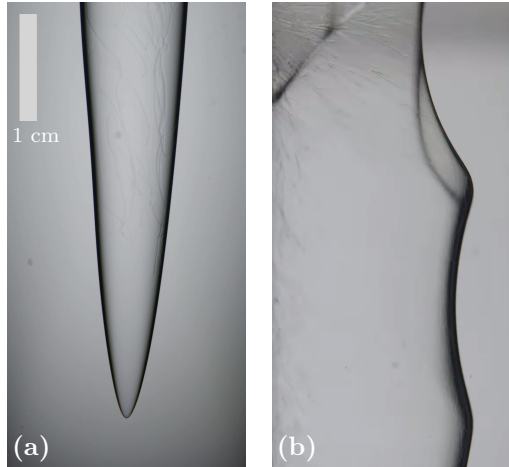


FIGURE 2: Close-up images of ice during experiments at (a) $T_\infty = 4^\circ\text{C}$ and (b) $T_\infty = 6^\circ\text{C}$. For $T_\infty = 4^\circ\text{C}$ we find the ice sharpens from below, while at $T_\infty = 6^\circ\text{C}$ it develops scallops.

mathematical models. Experiments strip away mathematical complications, providing a direct avenue to the full moving boundary problem, while simulations allow us to perform systematic parameter studies. In this section, we review our experimental and numerical frameworks and provide an overview of some results. Throughout our study, we are primarily interested in characterizing the effects of the far-field temperature T_∞ , which determines the level of influence the density inversion has on the flow.

Table-top geophysics

As a laboratory model of an iceberg, we consider a cylinder of ice, approximately 20cm tall, submerged in a tank of water maintained at temperature T_∞ . To control T_∞ , we work in a cold room, typically used for biological research, which has operating temperatures in the range $0 - 10^\circ\text{C}$.

Our experiments reveal three primary classes of dynamics. At higher temperatures, $T_\infty > 8^\circ\text{C}$, we find the ice sharpens from the top, analogous to what has recently been discovered during dissolution [2]. To understand this analogy, note that in this regime the dimensionless ice temperature $\theta_0 = (T_0 - T_*) / (T_\infty - T_0)$ approaches zero and the dimensionless far-field temperature $\theta_\infty = (T_\infty - T_*) / (T_\infty - T_0)$ approaches one. In terms of the buoyancy force $Ra\theta^2$, this means cold fluid near the ice surface is less buoyant, or heavier, than warm fluid away from the surface, just as saturated water near a dissolving body is heavier than fresh water away from it. In both these cases, the difference in buoyancy forces at the surface and the far-

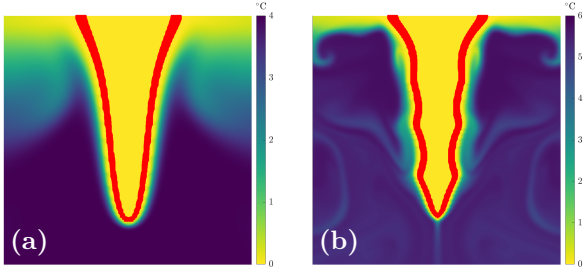


FIGURE 3: Temperature fields from a 2D phase-field simulation with (a) $T_\infty = 4^\circ\text{C}$ and (b) $T_\infty = 6^\circ\text{C}$. The yellow region denotes the ice where $T = 0^\circ\text{C}$, and the red curve denotes the phase boundary $\phi = 1/2$.

field causes the fluid near the surface to sink, which sharpens the body from the top.

At low temperatures, $T_0 < T_\infty < T_*$, we discover the ice also sharpens, but this time from the bottom (Figure 2a). The mechanism here is similar to the previous case. In this temperature range, the dimensionless melting temperature θ_0 is now larger in magnitude than the dimensionless far-field temperature θ_∞ , meaning the buoyancy force $\text{Ra}\theta^2$ is stronger near the surface than in the far-field. This causes lighter fluid near the surface to rise, opposite to before, which sharpens the ice from the bottom. This inverse sharpening is a typical characteristic of icebergs, both in the form of large pinnacles (Figure 1b), as well as smaller ridges (Figure 1c).

In between these regimes, when $T_* < T_\infty < 8^\circ\text{C}$, something very different occurs. Instead of strictly upward or downward flow, we find the flow near the ice consists of adjacent regions of rising and sinking fluid. This shear flow drives an instability, which carves wave-like patterns into the ice surface (Figure 2b), similar to scallops found on icebergs. Such patterns are known to form under imposed flow, but our experiments demonstrate they can be created by buoyancy forces alone.

In this intermediate range, fine-tuning the far-field temperature T_∞ can be challenging, so to gain further insight we turn to numerical simulation.

Numerical methods

Numerical methods for moving boundary problems are generally classified as interface-tracking or fixed-grid methods. In interface-tracking methods, the melting body is explicitly parametrized and then related to the fluid, typically by deforming the computational grid [6] or using an immersed boundary type method [7]. These methods can resolve fine-scale features on the interface, but are often computationally

intensive. Fixed grid methods, on the other hand, use a thermodynamic model for phase change, which typically appears as a source term in the temperature equation. The PDEs can then be solved on a standard Cartesian grid, making it easy to incorporate melting dynamics into existing fluid solvers.

One of the most popular fixed-grid methods is the phase-field method [8] [9], which we use in this study. Starting from the Stefan condition (3), one can derive a nonlinear diffusion equation for a phase parameter ϕ , which couples to the velocity and temperature equations (2a) and (2c). In this framework, ϕ ranges smoothly between the solid ($\phi = 0$) and liquid ($\phi = 1$) phases, leading to higher regularity in the solution and therefore better overall accuracy compared to other fixed grid methods.

Snapshots of the temperature field from our phase-field simulations at $T_\infty = 4^\circ\text{C}$ and $T_\infty = 6^\circ\text{C}$ are shown in Figure 3. The ice is represented by the solid yellow region, outlined by the phase boundary $\phi = 1/2$ in red. At $T_\infty = 4^\circ\text{C}$, the ice sharpens from the bottom, while at $T_\infty = 6^\circ\text{C}$ it forms scallops on the surface. This behavior is in agreement with the experimental results from Figure 2, with similar tip curvatures and scallop wavelengths.

To summarize, our experiments and simulations reveal three distinct shape regimes: sharpening from below ($T_0 < T_\infty < T_*$), sharpening from above ($T_\infty > 8^\circ\text{C}$), and scalloping ($T_* < T_\infty < 8^\circ$). These observations suggest several modeling approaches, which we describe in the next section.

MODELING

In this section we propose two analytical models to quantify our experimental and numerical observations. The first model, based on boundary layer theory, characterizes the sharpening behavior, while the second, based on linear stability analysis, describes the scalloping patterns.

Boundary layer theory

Boundary layer theory is a useful tool for analyzing moving boundary problems coupled to flows [10] [11]. First, we assume the flow is two-dimensional and introduce a body fitting coordinate system (x, y) , where $x = 0$ corresponds to the tip of the ice. In this coordinate system, the ice surface can be parametrized by the angle $\alpha(x)$ made between the tangent line to the surface and the horizontal axis. Next, assuming the flow is steady, unidirectional, and localized near the ice surface, it can be shown that the Boussinesq equa-

tions (2a)–(2c) asymptotically reduce to the *boundary layer equations*,

$$\begin{aligned} uu_x + vv_y &= \text{Pr} \left[u_{yy} + \text{Ra}(\theta^2 - \theta_\infty^2) \sin \alpha(x) \right], \\ u\theta_x + v\theta_y &= \theta_{yy}, \\ u_x + v_y &= 0. \end{aligned} \quad (4)$$

In this formulation u and v are the fluid velocity tangent and normal to the surface, respectively, and θ is the temperature, non-dimensionalized as before.

Introducing a similarity variable $\eta(x, y)$, which depends on the Rayleigh number, the Prandtl number, and the tangent angle $\alpha(x)$, the boundary layer equations (4) can be transformed into two coupled ordinary differential equations (ODEs) for a similarity-stream function $f(\eta)$ and similarity temperature $h(\eta)$,

$$\begin{aligned} f''' + 3ff'' - 2f'^2 + (h^2 - \theta_\infty^2) &= 0, \\ h'' + 3\text{Pr}fh' &= 0. \end{aligned}$$

From these ODEs, the normal velocity of the ice-water interface can be computed explicitly by evaluating $\partial\theta/\partial y = h'(\eta)\partial\eta/\partial y$ at the surface $y = 0$ and using the Stefan condition (3),

$$v_n(x) = \text{St} \left(\frac{3\text{Ra}}{4\text{Pr}} \right)^{1/4} \frac{h'(0) \sin^{1/3} \alpha(x)}{\left(\int_0^x \sin^{1/3} \alpha(x') dx' \right)^{1/4}}.$$

Taylor expanding this expression near the tip $x = 0$ and using a curve-shortening equation for the tangent angle $\alpha(x)$, we can derive a power law for the tip curvature,

$$\kappa(t) = \kappa_0 \left(1 - \frac{t}{t_s} \right)^{-4/5}.$$

Notably, the negative exponent $-4/5$ on the right hand side of this equation indicates a finite-time singularity at t_s , which is a signature of the sharpening seen in the two regimes $T_0 < T_\infty < T_*$ and $T_\infty > 8^\circ\text{C}$. In reality, such singularities do not exist, and the Gibbs-Thomson effect limits their growth.

In the scalloping regime $T_* < T_\infty < 8^\circ\text{C}$, it seems the boundary layer solution is no longer valid, so a different approach is necessary.

Linear stability analysis

Wave formation is generally an indicator of linear instability. To analyze these instabilities, we typically look for a steady state solution and consider small perturbations about that state. As a basic model for flow near the ice surface, we consider a

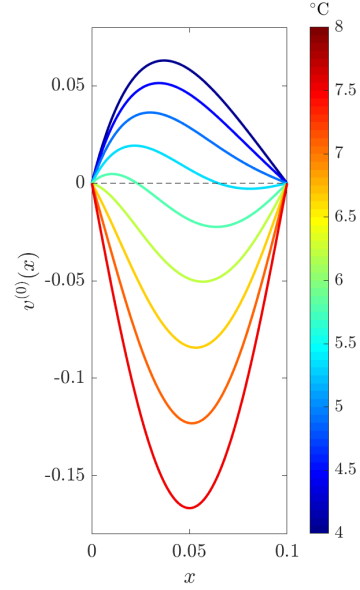


FIGURE 4: Steady state velocity profiles from linear stability analysis. For $5^\circ\text{C} < T_\infty < 6.5^\circ\text{C}$ the steady state exhibits both upward and downward flow in agreement with observations.

fluid, governed by the Boussinesq equations (2a) – (2c), confined between two vertical walls. We assume one wall is kept at the ice temperature θ_0 and the other at the far-field temperature θ_∞ . Assuming the vertical derivatives are small, there is a simple steady-state in this geometry, which we denote by $\mathbf{u}^{(0)} = (0, v^{(0)})$ and $\theta^{(0)}$. The vertical velocity profile $v^{(0)}$ is shown in Figure 4, demonstrating the bidirectional flow observed in experiments and simulations. Introducing the stream function ψ such that $\mathbf{u} = (\psi_z, -\psi_x)$ and perturbing the Boussinesq equations about the steady state $\psi = \psi^{(0)} + \varepsilon\hat{\psi}e^{ikz+\sigma t}$ and $\theta = \theta^{(0)} + \varepsilon\hat{\theta}e^{ikz+\sigma t}$, we get a generalized eigenvalue problem for the perturbation profiles $\hat{\psi}$ and $\hat{\theta}$, and their growth rate σ ,

$$\begin{aligned} \sigma(D^2 - k^2)\hat{\psi} - ikv_{xx}^{(0)}\hat{\psi} + ikv^{(0)}(D^2 - k^2)\hat{\psi} \\ = \text{Pr} \left[(D^2 - k^2)^2\hat{\psi} - 2\text{Ra}D(\theta^{(0)}\hat{\theta}) \right], \\ \sigma\hat{\theta} + ik\theta_x^{(0)}\hat{\psi} + ikv^{(0)}\hat{\theta} = (D^2 - k^2)\hat{\theta}, \end{aligned} \quad (5)$$

where $D = d/dx$. This eigenvalue problem, called the Orr-Sommerfeld equation, can provide insight into the wavelength of instability, its growth rate, and the way such properties vary with the far-field temperature. In particular, for all wavenumbers k that have an eigenvalue σ_* with positive real part, the perturbations will grow and the steady state $\mathbf{u}^{(0)}$ and $\theta^{(0)}$ becomes unstable.

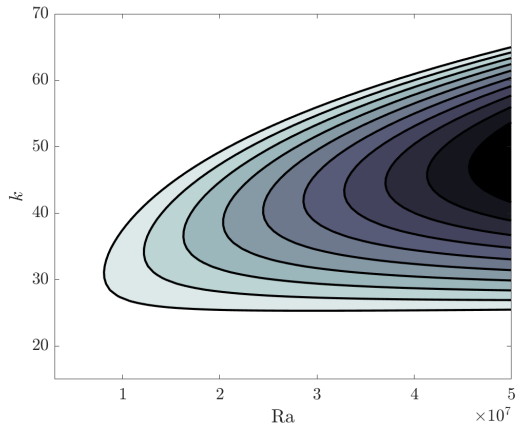


FIGURE 5: Region of unstable wavenumbers k versus the Rayleigh number for $T_\infty = 6^\circ\text{C}$. The shading indicates the growth rate of instability $\text{Re}(\sigma_*)$.

To solve the Orr-Sommerfeld equation (5), we expand the perturbation profiles $\hat{\psi}$ and $\hat{\theta}$ in a finite series of orthogonal basis functions, such as Chebyshev polynomials, and solve the corresponding eigenvalue problem for the system of coefficients. Figure 5 shows the computed region of unstable wavenumbers k versus the Rayleigh number for $T_\infty = 6^\circ\text{C}$. For the experimental conditions where we estimate $\text{Ra} \approx 2 \times 10^7$, this analysis predicts a scallop wavelength in the range 2–5cm, in rough agreement with the scallop from the experiment shown in Figure 2b.

OUTLOOK

The class of moving boundary problems is immense, and accelerating climate change is making them more relevant every day. The oceans are warming and polar ice is melting faster; the sea level is rising and coastal regions are eroding. Melting ice is just one part of this global process, and we hope to expand the tools we developed here to further understand other moving boundary problems related to climate change.

Throughout this study we assumed the ice was held fixed at the surface. In reality, as icebergs melt and change shape they can become gravitationally unstable and capsize. Polar scientists have noticed this is happening more often, and attribute the higher frequency to warmer waters. By generalizing our model to let the ice float freely, we can analyze the coupling between temperature, shape, and stability, as well as its impact on overall melt rates.

REFERENCES

- [1] Leif Ristroph. Sculpting with flow. *Journal of Fluid Mechanics*, 838, 2018.
- [2] Megan S. Davies Wykes, Jinzi Mac Huang, George A. Hajjar, and Leif Ristroph. Self-sculpting of a dissolvable body due to gravitational convection. *Physical Review Fluids*, 3, 2018.
- [3] Takeo Saioth. Natural convection heat transfer from a horizontal ice cylinder. *Applied Scientific Research*, 32, 1976.
- [4] Benjamin Gebhart and T. Wang. An experimental study of melting vertical ice cylinders in cold water. *Chemical Engineering Communications*, 13, 1982.
- [5] Srikanth Toppaladoddi and John S. Wettlaufer. Penetrative convection at high rayleigh numbers. *Physical Review Fluids*, 3, 2018.
- [6] Charles Puelz and Boyce Griffith. A sharp interface method for an immersed viscoelastic solid. *Journal of Computational Physics*, 409, 2020.
- [7] Jinzi Mac Huang, Michael J. Shelley, and David B. Stein. A stable and accurate scheme for solving the stefan problem with natural convection using immersed boundary smooth extension. *In progress*.
- [8] S.L. Wang, R.F. Sekerka, A.A. Wheeler, B.T. Murray, S.R. Coriell, R.J. Braun, and G.B. McFadden. Thermodynamically-consistent phase-field models for solidification. *Physica D*, 69, 1993.
- [9] B. Favier, J. Purseed, and L. Duchemin. Rayleigh b enard convection with a melting boundary. *Journal of Fluid Mechanics*, 858, 2018.
- [10] Jinzi Mac Huang, M. Nicholas J. Moore, and Leif Ristroph. Shape dynamics and scaling laws for a body dissolving in fluid flow. *Journal of Fluid Mechanics*, 765, 2015.
- [11] Matthew N. J. Moore, Leif Ristroph, Stephen Childress, Jun Zhang, and Michael J. Shelley. Self-similar evolution of a body eroding in a fluid flow. *Physics of Fluids*, 25, 2013.